JOURNAL OF BONE AND MINERAL RESEARCH
Volume 19, Number 4, 2004
Published online on January 12, 2004; doi: 10.1359/JBMR.040111

Brittle IV Mouse Model for Osteogenesis Imperfecta IV Demonstrates Postpubertal Adaptations to Improve Whole Bone Strength

Kenneth M Kozloff,[1] Angela Carden,[2] Clemens Bergwitz,[3] Antonella Forlino,[3] Thomas E Uveges,[3] Michael D Morris,[2] Joan C Marini,[3] and Steven A Goldstein[1]

ABSTRACT: The Brtl mouse model for type IV osteogenesis imperfecta improves its whole bone strength and stiffness between 2 and 6 months of age. This adaptation is accomplished without a corresponding improvement in geometric resistance to bending, suggesting an improvement in matrix material properties.

Introduction: The Brittle IV (Brtl) mouse was developed as a knock-in model for osteogenesis imperfecta (OI) type IV. A Gly349Cys substitution was introduced into one *col1a1* allele, resulting in a phenotype representative of the disease. In this study, we investigate the effect of the Brtl mutation on whole bone architecture, strength, and composition across a range of age groups.
Materials and Methods: One-, 2-, 6-, and 12-month-old Brtl and wildtype (WT) mice were analyzed. Femurs were assessed at the central diaphysis for cortical geometric parameters using μCT and were subsequently mechanically tested to failure by four-point bending. Matrix material properties were predicted using μCT data to normalize data from mechanical tests. Raman spectroscopy and DXA were used to assess matrix composition.
Results: Our findings show a postpubertal adaptation in which Brtl femoral strength and stiffness increase through a mechanism independent of changes in whole bone geometry. These findings suggest an improvement in the material properties of the bone matrix itself, rather than improvements in whole bone geometry, as seen in previous mouse models of OI. Raman spectroscopic results suggest these findings may be caused by changes in mineral/matrix balance rather than improvements in mineral crystallinity.
Conclusions: Our findings parallel the currently unexplained clinical observation of decreased fractures in human OI patients after puberty. The Brtl mouse remains an important tool for investigating therapeutic interventions for OI.
J Bone Miner Res 2004;19:614–622. Published online on January 12, 2004; doi: 10.1359/JBMR.040111

Key words: biomechanics, osteogenesis imperfecta, collagen, knock-in, mouse model

INTRODUCTION

OSTEOGENESIS IMPERFECTA (OI) is an autosomal dominant genetic disorder of the extracellular matrix.[1,2] The hallmark feature of OI is bone fragility and susceptibility to fracture from minimal trauma. Patients with OI are customarily grouped in types I to IV, according to the Sillence classification, based on clinical and radiographic features.[1] About 90% of OI cases are caused by mutations in type I collagen, the major structural component of the extracellular matrix of bone and skin. The severity of the disorder is related to the location and type of mutation in each collagen alpha chain. Recently, a small percentage of OI patients (about 10%) have been reclassified as types V-VII based on skeletal histology and radiographic features; these cases do not result from collagen mutations.[3–6] Type IV OI is the moderately severe form of the disorder, with phenotypes ranging between the milder phenotype of OI type I and the more severe complications of OI type III.[1] Infants are often born with fractures, but fracture rate can be quite variable throughout childhood.[1] Interestingly, patients with type IV OI show a marked decrease in fracture rate near the age of puberty,[1,7] suggesting the existence of an unidentified adaptation mechanism which increases whole bone structural integrity.

Although rearrangements and exon skipping mutations have been described, OI type IV typically (85%) results from a glycine substitution in one of the collagen I chains.[1] Understanding how a single point mutation in the collagen gene can alter the susceptibility of an entire bone to fracture requires observations over multiple hierarchical levels of the tissue. Furthermore, the development of effective therapeutic agents for OI may require manipulation at one or more of these hierarchical levels. Thus, a critical examination of an appropriate and reproducible model for OI is required.

The authors have no conflict of interest.

[1]Orthopaedic Research Laboratories, Department of Orthopaedic Surgery, University of Michigan, Ann Arbor, Michigan, USA; [2]Department of Chemistry, University of Michigan, Ann Arbor, Michigan, USA; [3]Bone and Extracellular Matrix Branch, National Institute of Child Health and Human Development, Bethesda, Maryland, USA.

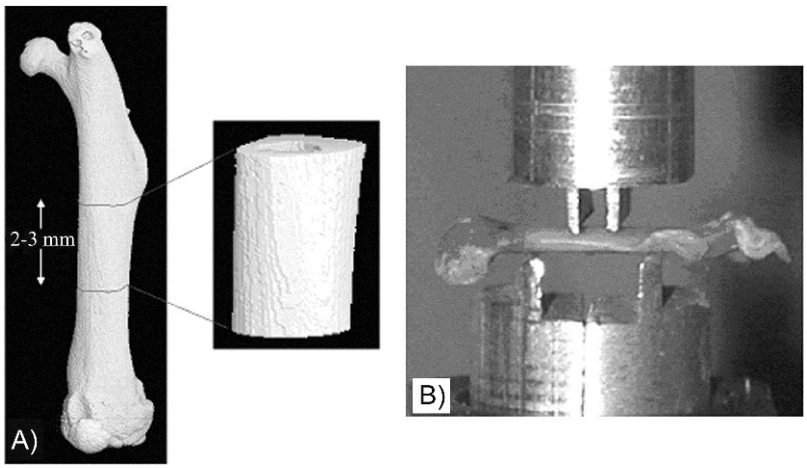

FIG. 1. (A) μCT image of central diaphyseal region of analysis. (B) Femurs were subjected to four-point bending with the posterior surface under tension.

Several murine models of OI have been reported,[8–11] however, none of these mice result from dominant negative transmission of a typical glycine substitution mutation. Only naturally occurring and knock-in mutations will have both the physiological tissue distribution of the mutant collagen transcripts and the physiological levels of mutant alpha chain, because their expression is under the control of endogenous promoters. For these reasons, the Brittle IV, or Brtl mouse, was developed as the first knock-in murine model for OI.[12] Brtl is heterozygous for a Gly349→Cys (G349C) substitution in one *col1a1* allele, reproducing the genetic mutation found in a type IV child.[13] Brtl mice show a moderately severe skeletal phenotype, with long bone deformities and bone fragility. Furthermore, the Brtl mouse reproduces the molecular, biochemical, and radiographic features of OI type IV,[12] making it an excellent model for studying this disease.

The purpose of this investigation was to evaluate the effects of a single glycine substitution in the alpha 1(I) collagen chain on the whole bone properties of the Brtl mouse model for OI. This involves examination of the inherent material properties of the bone matrix, the relative levels of mineral and extracellular matrix constituencies, and the structural organization of the femur. In addition, these studies were performed in mice over a range of ages, from skeletally immature to mature adult, to observe any changes in parameters over time.

MATERIALS AND METHODS

Specimens

Seventy nine male Brtl and WT mice were killed at 1 (Brtl, $n = 10$; WT, $n = 14$), 2 (Brtl, $n = 10$; WT, $n = 12$), 6 (Brtl, $n = 11$; WT, $n = 12$), and 12 (Brtl, $n = 5$; WT, $n = 5$) months of age, corresponding to developmental status of childhood, puberty, mature young adult, and adult. Brtl mice have a mixed background of Sv129/CD-1/C57BL/6S and are bred by crossing heterozygous Brtl with WT, each generated through separate Brtl $\times$ WT matings.[12] After death, femurs were harvested, stripped of soft tissue, and stored frozen in saline until ready for testing. In one-half of the specimens, left femurs were analyzed for geometric properties, and right femurs were mechanically tested. In the remainder of the population, bone geometry and mechanical properties were both measured in left femurs. In a subpopulation of 11 mice, both femurs were evaluated to assess left-right differences in structural properties. A separate group of 43 Brtl and WT mice were used to determine BMD of the left femur. All experiments were performed in accordance with approval from the NICHD ACUC committee.

Evaluation of femoral geometry by μCT

A custom μCT scanner developed and validated in our laboratory[14–16] was used to scan femurs at 25-mm voxel resolution to assess geometric properties of the central diaphysis (Fig. 1A). The 3D data set generated by μCT is organized as a series of slices 25 μm thick, oriented along the long axis of the bone. A threshold was applied to each slice,[15] and transverse cross-sections were analyzed over 2 (1 month) or 3 mm (2, 6, and 12 months) segments starting at the distal insertion of the third trochanter and extending toward the distal end of the bone. Each slice was analyzed for its cross-sectional area, cortical thickness, and bending moment of inertia in the anterior-posterior direction about the medial-lateral axis. Data within each femur was averaged over the 2- or 3-mm segment to provide representative values over the entire 3D mid-diaphysis.

Whole bone mechanical properties

Femurs were loaded to failure in four-point bending at 0.5 mm/s in the anterior-posterior direction using a servohydraulic testing machine (810 Material Test System; MTS Systems Corporation, Eden Prairie, MN, USA; Fig. 1B). Regions loaded in four-point bending corresponded to those measured by μCT. Load head displacement was monitored using an external linear variable differential transducer (LVDT; Lucas Schavitts, Hampton, VA, USA), and load data were collected with a 50-lb load cell (Sensotec, Columbus, OH, USA). Data were sampled at 200 Hz on a Macintosh IIci computer through an A/D system (Labview; National Instruments, Austin, TX, USA). Load-

displacement curves were analyzed for whole bone yield load, stiffness, yield energy, maximum load, failure energy, and post-yield displacement.

Predicted matrix properties

Results obtained from whole bone mechanical tests are influenced by the material properties of the bone matrix, as well as by the structural organization of the whole bone. Therefore, to separate the relative contribution of matrix material properties from whole bone structural organization, material properties of the extracellular matrix were predicted using beam theory[17] based on the geometric properties of the femur measured by μCT. Predicted ultimate stress is assumed to be greatest at the posterior surface, which is the area under greatest tension during bending experiments, and is calculated as

$$\sigma = \frac{Fac}{2I} \quad (1)$$

whereas the equation for predicted elastic modulus is

$$E = S\,\frac{a^2}{12I}(3L - 4a) \quad (2)$$

where F equals the measured maximum load, c is the distance from the centroid of the bone to the posterior periosteal surface, I is the moment of inertia of bending in the anterior-posterior direction, S is the initial stiffness of the bone, and L and a are geometric constants based on the four-point bending setup (3.57 and 0.99 mm).

These equations predict inherent material properties of the extracellular matrix, assuming a bending mode of failure.

Raman spectroscopy

Vibrational spectroscopy is ideal for probing the material properties of biological specimens nondestructively.[18] Both Raman and infrared spectroscopy yield simultaneous information about both the inorganic and organic components of bone, yet leave the specimen intact for further testing. Because it is a light scattering measurement, Raman spectroscopy is especially advantageous for the thick specimens used in this study. An epi-illumination excitation/collection optical configuration is used, and specimens do not have to be transparent. As a preliminary investigation into the collagen-mineral ultrastructure of the Brtl bone matrix, 12 specimens from 2- and 6-month-old animals (n = 3 per group) were prepared for Raman spectroscopic imaging from contralateral femurs by using a custom micromilling device to create barbell-shaped specimens.[19–21] Gauge sections were ~200 × 300 μm in cross-section and 1000 μm long.

The Raman imaging system has been previously described.[22–25] Raman scatter was excited using a high-aspect ratio rectangular laser beam at 785 nm (Kaiser Optical Systems). The total laser power at the specimen surface was ~150 mW. The beam was focused onto the center of the specimen's gauge length through a 10×/0.5 NA objective (Zeiss), and the resulting Raman scatter was collected in an epi-illumination mode through the same objective. In this manner, Raman spectra were excited at every point along the ~200-μm-long laser rectangle. The Raman scatter was focused into an axial-transmissive spectrograph (Kaiser Optical Systems) and detected using a thermoelectrically cooled CCD detector (Andor Technologies). To increase the number of spectra available for analysis, the specimen was translated in 1-μm steps using a computer-controlled X-Y translation stage (New England Affiliated Technologies), and a new line of spectra was acquired at each new specimen position. This was repeated 10 times for each specimen, creating a small Raman image ~184 × 11 μm in size and containing a total of 1260 Raman spectra. The total acquisition time for each image was ~50 minutes. Specimens were kept frozen before and after these experiments.

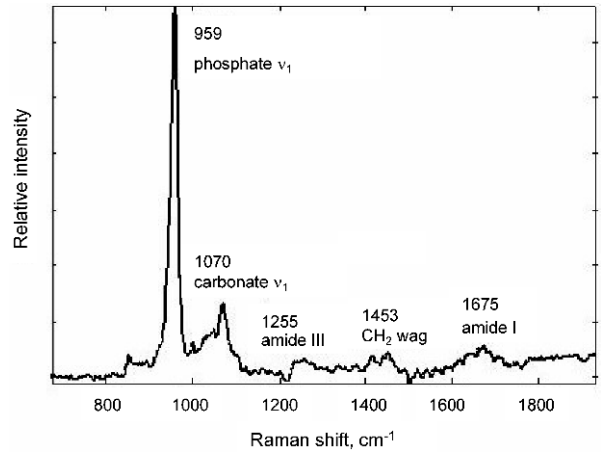

FIG. 2. Raman spectrum of a 6-month-old WT mouse femur. Important bands discussed in this paper are indicated together with their vibrational assignments. The amide II, CH_2 wag, and amide I bands result from vibrations of the collagenous matrix, whereas the phosphate υ_1 and carbonate υ_1 bands arise from the bone mineral.

Two different approaches were used for the analysis of the Raman spectroscopic data. A multivariate approach known as factor analysis[26,27] was used to determine whether different types of mineral and/or collagenous matrix were present within the areas imaged. This methodology is used to extract Raman spectra from large data sets, such as the hyperspectral images presented here. The details of application to bone tissue spectra have been previously reported.[28,29] Differences in mineral or organic matrix composition affect the Raman spectrum in subtle but observable ways. If the composition of the mineral and/or matrix varies across the area imaged, factor analysis is able to separate the spectra of the different mineral and/or matrix species. Thus, multiple mineral or matrix species, each represented by its own Raman spectrum, may be observed within a single image area. Alternatively, if there is no variation in mineral and/or matrix composition within the area imaged, only a single mineral and/or matrix species will be observed. Univariate analysis, in the form of band height ratios, was also performed on the Raman spectra, a

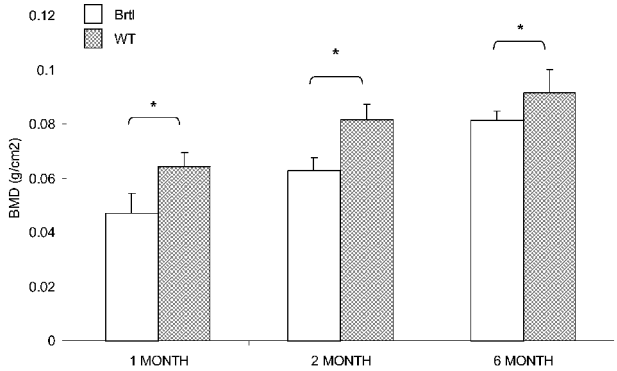

FIG. 3. Brtl femoral areal BMD is significantly less than WT at each age (*$p < 0.05$). Additionally, the gain in Brtl aBMD between 2 and 6 months of age is significantly greater than that of WT (*$p < 0.05$).

sample of which is shown in Fig. 2. Carbonate-to-phosphate ratios were computed from the υ_1 band heights of the relative carbonate (~1070 cm^{-1}) and phosphate (~959 cm^{-1}) peaks. Full-width half-maximum (FWHM) values of the υ_1 phosphate band were calculated to provide a qualitative indication of the quality, or crystallinity, of the mineral phase.[30,31] Representative mineral-to-matrix ratios were calculated by ratioing the height of the phosphate peak to the height of the amide I peak (~1675 cm^{-1}).

Evaluation of aBMD by Piximus

Male mice aged 1 (Brtl, $n = 5$; WT, $n = 5$), 2 (Brtl, $n = 7$; WT, $n = 8$), and 6 (Brtl, $n = 9$; WT, $n = 8$) months were killed by lethal injection. Areal BMD (aBMD) scans of Brtl mouse femurs were compared with those of age-matched, littermate controls using a GE Lunar PIXImus2 (Madison, WI, USA) on the whole mouse specimen and the internal calibration standards provided by GE.

Statistical analysis

μCT and four-point bending data were statistically analyzed using multivariate general linear models for each age group, with significance attributed to $p < 0.05$. A nonparametric repeated measures model (Wilcoxon signed-rank test) was used to test for within-mice differences in the subset of μCT data. Raman spectra were analyzed using factor analysis to identify numbers of mineral and organic species in the matrix. Univariate analysis was performed for phosphate to carbonate ratios and measures of full width half-maximum of the υ1 phosphate band. aBMD values of Brtl and WT age-matched littermates were analyzed using a Mann-Whitney U with exact significances test for genotypic differences, and differences in BMD gain between 2 and 6 months were assessed using a general linear model and testing for interactions between age and genotype. Data are presented as mean ± SD.

RESULTS

aBMD of Brtl femurs

Figure 3 shows a comparison of left femoral bone densities of male Brtl femurs and WT counterparts. At 1, 2, and 6 months of age, Brtl femurs have significantly lower aBMD than WT. Both genotypes show significant increases in aBMD at each age point; however, Brtl significantly improves its rate of mineralization from 72.8% and 76.2% of WT values at 1 and 2 months of age, respectively, to 88.9% of WT aBMD at 6 months of age ($p < 0.05$).

TABLE 1. GEOMETRIC PARAMETERS DERIVED FROM μCT

Age	*Genotype*	*Cross-sectional area (mm^2)*	*Cortical thickness (mm)*	*n*
1 Month	Brtl	0.58 ± 0.11*	0.16 ± 0.02*	8
	WT	0.73 ± 0.09	0.19 ± 0.02	13
2 Month	Brtl	0.75 ± 0.07*	0.20 ± 0.02*	10
	WT	1.05 ± 0.11	0.24 ± 0.03	12
6 Month	Brtl	1.03 ± 0.17*	0.28 ± 0.04	11
	WT	1.26 ± 0.23	0.28 ± 0.04	12
12 Month	Brtl	1.18 ± 0.20	0.26 ± 0.05	5
	WT	1.22 ± 0.13	0.26 ± 0.04	5

Values are means ± SD.
*$p < 0.05$; Brtl vs. WT.

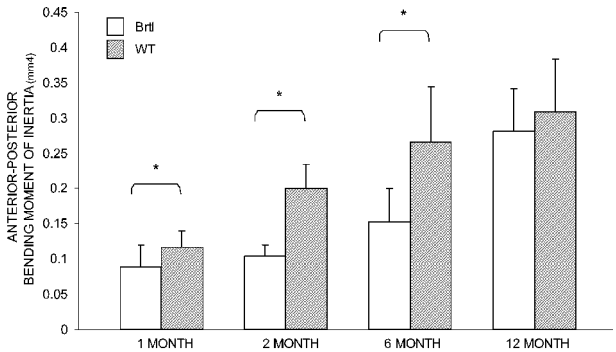

FIG. 4. Bending moments in the anterior-posterior direction show that the structure of the Brtl femur at 1, 2, and 6 months is less resistant to fracture than WT (*$p < 0.05$).

Intraspecimen variation in biomechanical studies

No significant differences were found between left and right femurs in the subset of mice analyzed by μCT. Therefore, where necessary, geometric data from left femurs were used to predict matrix material properties from right femoral four-point bending data in the same mouse. Two 1-month-old Brtl specimens were excluded from μCT analysis because of artifact during scanning. One 1-month-old Brtl specimen was fractured during the preload segment of loading and was excluded from the results.

Structural analysis

Results from μCT show that Brtl mouse femurs have significantly smaller cross-sectional areas at 1, 2, and 6 months than do their WT counterparts (Table 1). Cortical thickness values at 1 and 2 months were also significantly reduced (Table 1), but at the postpubertal age of 6 months, the Brtl mouse femur achieved parity with controls. Results from bending moments of inertia in the anterior-posterior direction (Fig. 4) show significant differences in Brtl com-

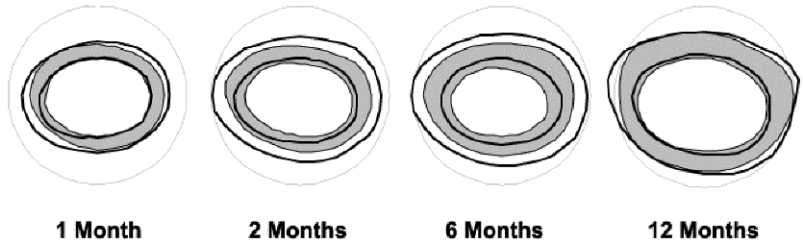

FIG. 5. Average cross-sectional views of WT femur diaphysis (heavy outline) superimposed on top of Brtl femur diaphysis (gray) (2-mm-diameter circle shown in light gray for reference). From left to right, 1, 2, 6, and 12 months.

TABLE 2. MECHANICAL PROPERTIES DERIVED FROM FOUR-POINT BENDING TESTS

Age	*Genotype*	*Post-yield displacement (mm)*	*Yield energy (N-mm)*	*Failure energy (N-mm)*	*Yield load (N)*
1 Month	Brtl	0.1946 ± 0.077*	0.27 ± 0.19 ($p = 0.087$)	1.90 ± 0.71*	6.11 ± 2.37*
	WT	0.3829 ± 0.138	0.51 ± 0.37	5.96 ± 2.06	9.26 ± 2.62
2 Month	Brtl	0.1759 ± 0.071*	0.32 ± 0.19	3.03 ± 1.49*	8.84 ± 1.85 ($p = 0.093$)
	WT	0.3016 ± 0.128	0.34 ± 0.20	7.37 ± 3.14	11.24 ± 3.93
6 Month	Brtl	0.1244 ± 0.056	0.55 ± 0.23*	3.96 ± 2.05	17.12 ± 3.85
	WT	0.1214 ± 0.88	1.15 ± 0.92	4.97 ± 3.33	22.67 ± 10.52
12 Month	Brtl	0.250 ± 0.014	0.63 ± 0.46	1.09 ± 0.71	17.81 ± 8.93
	WT	0.0572 ± 0.037	0.61 ± 0.18	2.16 ± 1.12	19.07 ± 5.46

Values are means ± SD.
*$p < 0.05$; Brtl vs. WT.

pared with controls at 1, 2, and 6 months. These results suggest that, based on structural geometry alone, independent of matrix-level material properties, the Brtl femur should be less resistant to an applied load than WT through 6 months of age. Average cross-sectional views shown in Fig. 5 summarize these results.

Mechanical testing

Femurs from young Brtl mice show a more brittle phenotype compared with WT, as shown by reduced post-yield displacement and reduced failure energy at 1 and 2 months (Table 2). Brtl mice show reduced yield (Table 2) and maximum loads (Fig. 6) at 1 and 2 months of age but equal WT values at 6 and 12 months. Brtl femurs are significantly less stiff at 2 months but comparable with WT at 6 and 12 months (Fig. 7). These findings show a postpubertal alteration whereby mechanical integrity of the femur is substantially improved to the level of the WT. These findings are contrary to geometric results from μCT, which suggested that based on structural geometry alone, Brtl mice at 6 months should be less stiff and less strong than WT. Therefore, we hypothesize that alterations occur in the Brtl matrix after puberty that dramatically improve the matrix material properties measured at 6 months of age.

Predicted matrix properties

When four-point bending results are normalized by bending moments of inertia to predict matrix material properties, predicted elastic modulus of the 6-month-old Brtl femur was significantly increased compared with WT (Table 3).

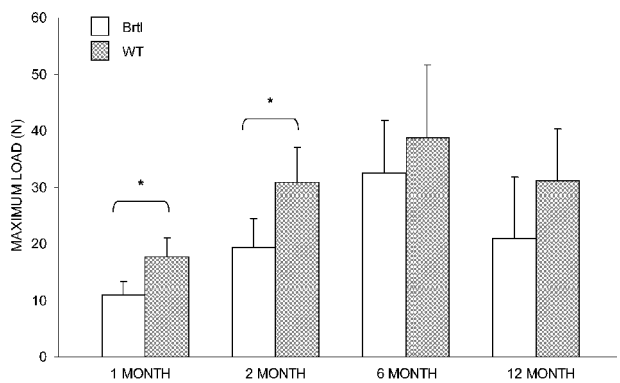

FIG. 6. Maximum load is reduced in Brtl femurs compared with WT at 1 and 2 months, while at 6 and 12 months, no significant differences were found. (* $p < 0.05$)

Additionally, 6-month-old Brtl femurs showed a strong trend toward increased predicted ultimate strength over WT ($p = 0.068$).

Raman spectroscopy

Predicted matrix properties suggest a dynamic period of alteration leading to increased material properties at the matrix level. To evaluate the potential mechanisms causing this change, specimens from 2- and 6-month-old animals were evaluated by Raman spectroscopy (Table 4). One 2-month-old Brtl specimen was dropped from the analysis

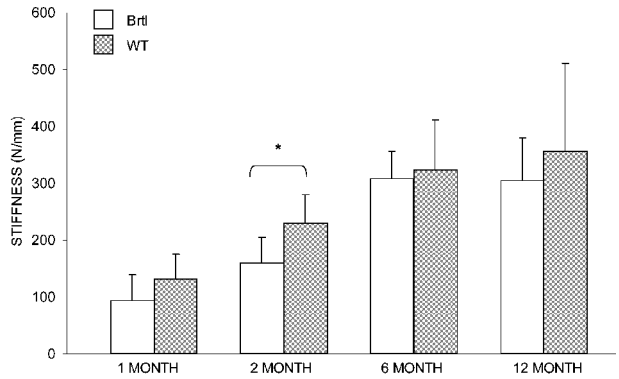

FIG. 7. Stiffness of the Brtl femur achieves equivalence to WT at 6 months of age.(* $p < 0.05$)

TABLE 3. PREDICTED ULTIMATE STRENGTH AND PREDICTED ELASTIC MODULUS

Age	*Genotype*	*Ultimate strength (MPa)*	*Elastic modulus (MPa)*
1 Month	Brtl	43.03 ± 10.28	612.65 ± 192.42
	WT	48.58 ± 7.21	624.98 ± 189.92
2 Month	Brtl	58.43 ± 12.12	862.44 ± 267.28
	WT	57.85 ± 12.66	645.24 ± 159.65
6 Month	Brtl	74.20 ± 22.27 ($p = 0.068$)	1180.99 ± 322.81*
	WT	58.33 ± 17.20	686.01 ± 133.9
12 Month	Brtl	29.83 ± 12.89	611.35 ± 147.15
	WT	44.04 ± 16.15	660.35 ± 268.39

Values are means ± SD.
* $p < 0.05$; Brtl vs. WT.

because of a poor signal-to-noise ratio, making baselining of the spectra difficult. One 6-month-old Brtl specimen was dropped from the analysis because of a failed Q-test. Analysis of both the mineral subregion and organic subregion of the Raman spectra revealed no trends in the number of mineral or matrix factors with respect to disease status. Six-month-old Brtl specimens seemed to have higher carbonate-to-phosphate ratios than WT specimens, and this trend was not evident at 2 months. Measures of phosphate υ_1 band width show no difference in mineral crystallinity with respect to age or disease state. However, results suggest that the Brtl mouse has a significantly reduced mineral-to-matrix ratio compared with WT at 6 months of age.

DISCUSSION

The Brtl mouse was generated as a model for OI type IV by introducing a classic glycine substitution in one *col1a1* allele.[12] Individuals with type IV OI have moderately severe skeletal fragility, with decreased fracture susceptibility after puberty. The Brtl mouse results presented here model the clinical course of the disorder in children. The femurs of prepubertal 1-month-old and pubertal 2-month-old Brtl mice were structurally less able to withstand a load than age-matched WT controls. This finding was verified through whole bone mechanical tests. At the postpubertal age of 6 months, however, the Brtl mouse femurs had whole bone strength and stiffness comparable with WT, despite having a bone geometrical organization less resistant to applied loads. Predicted material properties of elastic modulus and ultimate strength are increased, accounting for increases in whole bone strength through an increase in matrix-level material properties without corresponding structural adaptations. These findings are bolstered by results from the aBMD measurements. Brtl aBMD was significantly lower than WT at all ages; however, Brtl aBMD increased between 2 and 6 months at a rate greater than associated with the pubertal changes in WT mice. Raman results suggest a change in the balance of ultrastructural components, as mineral:matrix ratios adjust in Brtl from being nonsignificantly larger than WT at 2 months to being significantly lower at 6 months. The 2-month-old Raman data do not contradict the findings of reduced Brtl aBMD at all ages, because Raman measures the ratio, not total amount, of mineral and collagen constituencies at the ultrastructural level. If Brtl produces less collagen than WT at the ultrastructural level, it could still show a higher mineral:matrix ratio by Raman, but a lower aBMD because of the difference in the two measurement techniques.

Together, these findings suggest a period of adaptation between 2 and 6 months of age in which bone stiffness and strength attain WT values through a strengthening mechanism at the level of the extracellular matrix rather than through alterations in whole bone structural layout.

Significant further gains in bone strength are not demonstrated beyond 6 months of age. This finding is consistent with other studies showing minimal gains in bone strength and stiffness beyond 18 weeks of age in the C57BL/6J mouse[32] and constant peak torque between 6 and 12 months in C57BL/6J X C3H/He mice.[33] Furthermore, WT ductility is decreased at 6 and 12 months compared with earlier ages, rendering differences in failure energy and post-yield displacement no longer significant. This suggests a natural aging process in the WT mouse leading to age-related decreases in ductility. Similar decrements in femoral ductility have been shown in SAMR1 control mice and the SAMP6 mouse model for senile osteoporosis between 4 and 12 months of age.[34]

Other models of OI have demonstrated adaptations in response to a matrix-altering mutation. The Mov13 mouse carries a provirus preventing transcription of the α1(I) collagen gene.[35] Mice heterozygous for the Mov13 mutation show a 50% decrease in normal type I collagen and serve as a model for OI type I,[8] in which patients produce a reduced quantity of structurally normal type I collagen. At 8 weeks of age, Mov13 femurs are more brittle than WT because of microstructural differences between the two animals.[36] Furthermore, microbeams machined from the Mov13 femur show decreased matrix material properties and a reduced fatigue life compared with controls.[21] To compensate for these mechanical impairments, between the ages of 8 and 15 weeks, Mov13 mice deposit new bone matrix on the periosteal surfaces of the femur, significantly increasing their cortical area and bending moment of inertia.[37] This structural adaptation significantly improves the whole bone

Table 4. Results From Raman Spectroscopy Suggest an Alteration in Mineral-to-Matrix Ratios at 6 Months of Age

Age	*Genotype*	*Mineral factors*	*CO_3:PO_4 ratio*	*FWHM ν1 PO_4 band*	*Mineral/matrix ratio*
2 Month	Brtl	1, 1, 1	0.144 ± 0.011	16.25 ± 1.17	12.50 ± 4.79
	WT	1, 1, 1	0.162 ± 0.068	16.94 ± 0.46	8.45 ± 1.65
6 Month	Brtl	1, 2, 1	0.209 ± 0.027	17.15 ± 2.16	5.75 ± 0.11*
	WT	2, 1, 1	0.193 ± 0.056	17.13 ± 0.65	11.17 ± 2.99

* $p < 0.05$; Brt vs. WT.

bending strength of the Mov13 mouse to a level greater than control specimens.

The *oim/oim* mouse has a naturally occurring mutation that prevents pro-α2(I) chains from incorporating into type I collagen. The *oim/oim* extracellular matrix does not contain any normal type I collagen but is instead composed of α1(I) homotrimers.[9] This model for OI type III show reduced indices of whole bone strength compared with WT at all ages.[33,38] Whereas geometric-based indices of bone strength suggest an improved bone geometry in older *oim/oim* mice, this alteration fails to improve bone strength to the level of the WT femur.[33]

Our current findings show improvements in whole bone strength through improved matrix level material properties rather than geometrical adaptation. Raman spectroscopy was used as a means to investigate specific mineral-matrix interactions to help determine what alterations lead to the improvement in whole bone strength. Our results yielded no difference in number of mineral factors or mineral crystallinity with respect to disease state. Rather, a higher CO_3:PO_4 ratio and reduced mineral-to-matrix ratios were observed in 6-month-old Brtl specimens compared with WT. At this hierarchical level, it is unclear how these fundamental changes might affect the mechanical properties of the tissue. Bohic et al.[39] have shown similar increases in carbonation of tooth enamel from a patient with dentinogenesis imperfecta compared with an age-matched control. These findings differ from investigations in the *oim/oim* mouse. Camacho et al.[40] used Fourier-transform infrared spectroscopy, an imaging modality that provides similar information to Raman spectroscopy, to show differences in phosphate species[40] and crystallinity[38] compared with controls. *oim/oim* mice show trends opposite Brtl in CO_3:PO_4 and mineral:matrix ratios compared with the milder phenotype of *oim/+* at 6 months and compared with WT at 1 year.[40] Differences in these findings may be because of differences in the collagen defect. Matrix containing only α1(I) homotrimeric molecules in the *oim/oim* mice may induce a different mineralization template than formed by Brtl matrix, which contains a mixture of normal collagen and mutant collagen with a glycine to cysteine substitution. Neither Mov13 nor *oim/oim* mice show a compensatory mechanism at the level of the extracellular matrix capable of significantly improving whole bone mechanical strength to the level of controls, independent of changes in whole bone geometry. The femur of the Brtl mouse demonstrates this type of alteration.

Vetter et al.[41] have demonstrated small but significant decreases in apatite crystal size in children and adolescents with type IV OI compared with controls. In the current study, no changes in mineral crystallinity were found between Brtl and WT mice; however, we cannot definitively rule out this possibility because no studies have yet calibrated Raman band width to mineral crystallinity as measured by X-ray diffraction.

Another limitation to this study is the small sample size used in the Raman analysis. Additionally, milling of the microspecimens may have introduced artifact because of mechanical deformation of the bone.[22,25] Further analysis of the Brtl extracellular matrix is warranted. Changes in tissue microarchitecture, such as percent porosity and relative balance of woven versus lamellar bone, have been demonstrated to be important mediators of mechanical behavior in the Mov13 mouse.[36] Alterations in porosity or remodeling spaces, as seen in human cases of OI, may lead to the inclusion or deduction of stress risers within the bone matrix, which would be unaccounted for in our current calculations for predicted strength and modulus. Furthermore, woven and lamellar bone distribution may change as Brtl ages, altering the mechanical profile of the bone. In addition to microarchitecture, further investigation of the mineral and organic phase of the Brtl bone through methods such as small-angle X-ray scattering[42] and transmission electron microscopy[43] may lend insight into mineral crystal size, shape, orientation, and arrangement within the matrix. These methods may be needed to lend further understanding into the results generated through Raman spectroscopy.

Results from this study and others[37] suggest two general avenues of therapeutics for the disease: (1) improving geometric resistance to fracture, as in the Mov13 mouse, and (2) improving the material properties of the extracellular matrix itself, as shown here in the Brtl mouse. Hormones such as parathyroid hormone (PTH) or other anabolic drugs may be useful as a means of improving geometric resistance to fracture by adding bone to the cortex as seen in both animal[44,45] and human[46] histomorphometric studies. Bisphosphonates have been hypothesized to change the material properties of bone, possibly through increases in secondary matrix mineralization.[47–49] Indeed, alendronate, a third-generation bisphosphonate, has been demonstrated to reduce the number of fractures and increase femoral metaphyseal density in the growing *oim/oim* mouse model for OI.[50] The Brtl mouse is an appropriate model in which to address these two avenues of therapeutics and their potential implications on OI bone mechanics and geometry.

The findings presented here parallel clinically observed decreases in OI patient fracture rate after puberty without

administration of drug therapies.[7] The mechanism of this improvement in patient bone integrity is not well understood. The postpubertal decrease in fracture rate occurs with both glycine substitutions and exon skipping defects of collagen. Our results are the first to suggest a possible matrix-level adaptation leading to improved whole bone strength without corresponding increases in structural geometry in a model of OI. It is apparent that nature has developed mechanisms to adapt whole bone integrity to the fragility induced by type I collagen mutations. Further investigations are underway to determine the molecular mechanisms triggering this adaptation in Brtl matrix properties and the nature of the changes in postpubertal matrix composition. Exploiting these naturally occurring adaptation strategies may provide novel therapeutic interventions for OI.

ACKNOWLEDGMENTS

This study was supported by National Institutes of Health AR46024 (SAG), National Institutes of Health AR47969 (MDM) and NICHD, National Institutes of Health Intramural Funding (JCM). KMK is supported by a Whitaker Foundation Graduate Student Fellowship. We thank EP Frankenburg, M Spurchise, R Rae Jr, J Hall, S Volkmann, D Kayner and C Roehm for their valuable contributions to this study.

REFERENCES

1. Byers PH 2002 Osteogenesis imperfecta. In: Royce PM, Steinmann B (eds.) Connective Tissue and Its Heritable Disorders, 2nd ed. Wiley-Liss, Inc., New York, NY, USA, pp. 385–430.
2. Kuivaniemi H, Tromp G, Prockop DJ 1991 Mutations in collagen genes: Causes of rare and some common diseases in humans. FASEB J **5:**2052–2060.
3. Glorieux FH, Rauch F, Plotkin H, Ward L, Travers R, Roughley P, Lalic L, Glorieux DF, Fassier F, Bishop NJ 2000 Type V osteogenesis imperfecta: A new form of brittle bone disease. J Bone Miner Res **15:**1650–1658.
4. Labuda M, Morissette J, Ward LM, Rauch F, Lalic L, Roughley PJ, Glorieux FH 2002 Osteogenesis imperfecta type VII maps to the short arm of chromosome 3. Bone **31:**19–25.
5. Ward LM, Rauch F, Travers R, Chabot G, Azouz EM, Lalic L, Roughley PJ, Glorieux FH 2002 Osteogenesis imperfecta type VII: An autosomal recessive form of brittle bone disease. Bone **31:**12–18.
6. Glorieux FH, Ward LM, Rauch F, Lalic L, Roughley PJ, Travers R 2002 Osteogenesis imperfecta type VI: A form of brittle bone disease with a mineralization defect. J Bone Miner Res **17:**30–38.
7. Marini JC 1988 Osteogenesis imperfecta: Comprehensive management. Adv Pediatr **35:**391–426.
8. Bonadio J, Saunders TL, Tsai E, Goldstein SA, Morris-Wiman J, Brinkley L, Dolan DF, Altschuler RA, Hawkins JE Jr, Bateman JF 1990 Transgenic mouse model of the mild dominant form of osteogenesis imperfecta. Proc Natl Acad Sci USA **87:**7145–7149.
9. Chipman SD, Sweet HO, McBride DJ Jr, Davisson MT, Marks SC Jr, Shuldiner AR, Wenstrup RJ, Rowe DW, Shapiro JR 1993 Defective pro alpha 2(I) collagen synthesis in a recessive mutation in mice: A model of human osteogenesis imperfecta. Proc Natl Acad Sci USA **90:**1701–1705.
10. Saban J, Zussman MA, Havey R, Patwardhan AG, Schneider GB, King D 1996 Heterozygous oim mice exhibit a mild form of osteogenesis imperfecta. Bone **19:**575–579.
11. Khillan JS, Olsen AS, Kontusaari S, Sokolov B, Prockop DJ 1991 Transgenic mice that express a mini-gene version of the human gene for type I procollagen (COL1A1) develop a phenotype resembling a lethal form of osteogenesis imperfecta. J Biol Chem **266:**23373–23379.
12. Forlino A, Porter FD, Lee EJ, Westphal H, Marini JC 1999 Use of the Cre/lox recombination system to develop a non-lethal knock-in murine model for osteogenesis imperfecta with an α1(I) G349C substitution. Variability in phenotype in BrtlIV mice. J Biol Chem **274:**37923–37931.
13. Sarafova AP, Choi H, Forlino A, Gajko A, Cabral WA, Tosi L, Reing CM, Marini JC 1998 Three novel type I collagen mutations in osteogenesis imperfecta type IV probands are associated with discrepancies between electrophoretic migration of osteoblast and fibroblast collagen. Hum Mutat **11:**395–403.
14. Feldkamp LA, Goldstein SA, Parfitt AM, Jesion G, Kleerekoper M 1989 The direct examination of three-dimensional bone architecture in vitro by computed tomography. J Bone Miner Res **4:**3–11.
15. Kuhn JL, Goldstein SA, Feldkamp LA, Goulet RW, Jesion G 1990 Evaluation of a microcomputed tomography system to study trabecular bone structure. J Orthop Res **8:**833–842.
16. Goulet RW 1993 The quantification of the structure and mechanical properties of trabecular bone. Ph.D. thesis, University of Michigan, Ann Arbor, MI.
17. Turner CH, Burr DB 1993 Basic biomechanical measurements of bone: A tutorial. Bone **14:**595–608.
18. Carden A, Morris MD 2000 Application of vibrational spectroscopy to the study of mineralized tissues. J Biomed Opt **5:**259–268.
19. Choi K, Goldstein SA 1992 A comparison of the fatigue behavior of human trabecular and cortical bone tissue. J Biomech **25:**1371–1381.
20. Kuhn JL, Goldstein SA, Choi K, London M, Feldkamp LA, Matthews LS 1989 Comparison of the trabecular and cortical tissue moduli from human iliac crests. J Orthop Res **7:**876–884.
21. Jepsen KJ, Schaffler MB, Kuhn JL, Goulet RW, Bonadio J, Goldstein SA 1997 Type I collagen mutation alters the strength and fatigue behavior of Mov13 cortical tissue. J Biomech **30:**1141–1147.
22. Carden A, Rajachar RM, Morris MD, Kohn DH 2003 Ultrastructural changes accompanying the mechanical deformation of bone tissue: A Raman imaging study. Calcif Tissue Int **72:**166–175.
23. Pezzuti JA, Morris MD, Bonadio JF, Goldstein SA 1998 Hyperspectral Raman imaging of bone growth and regrowth chemistry. Proc SPIE **3261:**270–276.
24. Timlin JA, Carden A, Morris MD, Bonadio JF, Hoffler CE, Kozloff KM, Goldstein SA 1999 Spatial distribution of phosphate species in mature and newly generated mammalian bone by hyperspectral Raman imaging. J Biomed Opt **4:**28–34.
25. Timlin JA, Carden A, Morris MD, Rajachar RM, Kohn DH 2000 Raman spectroscopic imaging markers for fatigue-related microdamage in bovine bone. Anal Chem **72:**2229–2236.
26. Malinowski ER 1991 Factor Analysis in Chemistry, 2nd ed. John Wiley & Sons, Inc., New York, NY, USA.
27. Reyment R, Joreskog KG 1996 Applied Factor Analysis in the Natural Sciences. Cambridge University Press, New York, NY, USA.
28. Morris MD, Crane NJ, Gomez LE, Ignelzi MA Jr 2004 Compatibility of staining protocols for bone tissue with Raman imaging. Calcif Tissue Int (in press).
29. Tarnowski CP, Ignelzi MA Jr, Morris MD 2002 Mineralization of developing mouse calvaria as revealed by Raman microspectroscopy. J Bone Miner Res **17:**1118–1126.
30. Freeman JJ, Wopenka B, Silva MJ, Pasteris JD 2001 Raman spectroscopic detection of changes in bioapatite in mouse femora as a function of age and in vitro fluoride treatment. Calcif Tissue Int **68:**156–162.
31. de Mul FF, Hottenhuis MH, Bouter P, Greve J, Arends J, ten Bosch JJ 1986 Micro-Raman line broadening in synthetic carbonated hydroxyapatite. J Dent Res **65:**437–440.
32. Ferguson VL, Ayers RA, Bateman TA, Simske SJ 2000 Development of endogenous osteoporosis in male C57BL/6J mice. J Bone Miner Res **15:**S461.
33. McBride DJ Jr, Shapiro JR, Dunn MG 1998 Bone geometry and strength measurements in aging mice with the oim mutation. Calcif Tissue Int **62:**172–176.
34. Silva MJ, Brodt MD, Ettner SL 2002 Long bones from the senescence accelerated mouse SAMP6 have increased size but reduced whole-bone strength and resistance to fracture. J Bone Miner Res **17:**1597–1603.
35. Schnieke A, Dziadek M, Bateman J, Mascara T, Harbers K, Gelinas R, Jaenisch R 1987 Introduction of the human pro alpha 1(I) collagen gene into pro alpha 1(I)-deficient Mov-13 mouse cells leads to formation of functional mouse-human hybrid type I collagen. Proc Natl Acad Sci USA **84:**764–768.

36. Jepsen KJ, Goldstein SA, Kuhn JL, Schaffler MB, Bonadio J 1996 Type-I collagen mutation compromises the post-yield behavior of Mov13 long bone. J Orthop Res **14:**493–499.
37. Bonadio J, Jepsen KJ, Mansoura MK, Jaenisch R, Kuhn JL, Goldstein SA 1993 A murine skeletal adaptation that significantly increases cortical bone mechanical properties. Implications for human skeletal fragility. J Clin Invest **92:**1697–1705.
38. Camacho NP, Hou L, Toledano TR, Ilg WA, Brayton CF, Raggio CL, Root L, Boskey AL 1999 The material basis for reduced mechanical properties in oim mice bones. J Bone Miner Res **14:**264–272.
39. Bohic S, Heymann D, Pouezat JA, Gauthier O, Daculsi G 1998 Transmission FT-IR microspectroscopy of mineral phases in calcified tissues. Comptes Rendus de l'Academie des Sciences Serie III, Sciences de la Vie **321:**865–876.
40. Camacho NP, Landis WJ, Boskey AL 1996 Mineral changes in a mouse model of osteogenesis imperfecta detected by Fourier transform infrared microscopy. Connect Tissue Res **35:**259–265.
41. Vetter U, Eanes ED, Kopp JB, Termine JD, Robey PG 1991 Changes in apatite crystal size in bones of patients with osteogenesis imperfecta. Calcif Tissue Int **49:**248–250.
42. Fratzl P, Paris O, Klaushofer K, Landis WJ 1996 Bone mineralization in an osteogenesis imperfecta mouse model studied by small-angle x-ray scattering. J Clin Invest **97:**396–402.
43. McKee MD, Nanci A 1995 Postembedding colloidal-gold immunocytochemistry of noncollagenous extracellular matrix proteins in mineralized tissues. Microsc Res Tech **31:**44–62.
44. Hirano T, Burr DB, Turner CH, Sato M, Cain RL, Hock JM 1999 Anabolic effects of human biosynthetic parathyroid hormone fragment (1–34), LY333334, on remodeling and mechanical properties of cortical bone in rabbits. J Bone Miner Res **14:**536–545.
45. Wronski TJ, Yen CF 1994 Anabolic effects of parathyroid hormone on cortical bone in ovariectomized rats. Bone **15:**51–58.
46. Dempster DW, Cosman F, Kurland ES, Zhou H, Nieves J, Woelfert L, Shane E, Plavetic K, Muller R, Bilezikian J, Lindsay R 2001 Effects of daily treatment with parathyroid hormone on bone microarchitecture and turnover in patients with osteoporosis: A paired biopsy study. J Bone Miner Res **16:**1846–1853.
47. Chavassieux PM, Arlot ME, Reda C, Wei L, Yates AJ, Meunier PJ 1997 Histomorphometric assessment of the long-term effects of alendronate on bone quality and remodeling in patients with osteoporosis. J Clin Invest **100:**1475–1480.
48. Meunier PJ, Boivin G 1997 Bone mineral density reflects bone mass but also the degree of mineralization of bone: Therapeutic implications. Bone **21:**373–377.
49. Bourrin S, Ammann P, Bonjour JP, Rizzoli R 2002 Recovery of proximal tibia bone mineral density and strength, but not cancellous bone architecture, after long-term bisphosphonate or selective estrogen receptor modulator therapy in aged rats. Bone **30:**195–200.
50. Camacho NP, Raggio CL, Doty SB, Root L, Zraick V, Ilg WA, Toledano TR, Boskey AL 2001 A controlled study of the effects of alendronate in a growing mouse model of osteogenesis imperfecta. Calcif Tissue Int **69:**94–101.

Address reprint requests to:
Steven A Goldstein, PhD
Orthopaedic Research Laboratories
Department of Orthopaedic Surgery
University of Michigan
Room G-161
400 North Ingalls
Ann Arbor, MI 48109-0486, USA
E-mail: stevegld@umich.edu

Received in original form May 21, 2003; in revised form October 28, 2003; accepted November 14, 2003.